J. Synchrotron Rad. (1996). **3**, 101–111

A Foil-Mask Spectrometer for Laue Diffraction Pattern Imaging: Simultaneous Position, Intensity and Energy

Quentin S. Hanley, Darren R. Dunphy and M. Bonner Denton*

Department of Chemistry, University of Arizona, Tucson, AZ 85721, USA

(*Received 30 November 1995; accepted 7 March 1996*)

An X-ray spectrometer for simultaneous position, intensity and energy determinations suitable for Laue diffraction applications is described. The foil-mask spectrometer consists of a series of metal foils of varying composition and thickness which are used to modulate the energy distribution of an incident X-ray source. Three modes of operation are described: a high-resolution spectrometer for measurement of nearly monochromatic X-rays, an intensity discriminator for partitioning the intensity from a small number of spatially overlapped monochromatic X-ray sources, and a low-resolution spectrometer for polychromatic X-rays with broad spectral features. The first mode of operation is designed to allow the energy of monochromatic Laue reflections to be measured with a resolution suitable for determination of unit-cell parameters. The second mode of operation is designed to allow the intensity of each component in a spatial region containing overlapping orders or spatially overlapped reflections to be discriminated for use in refinements or space-group assignment. The third mode of operation is described for completeness. The theory behind each mode of operation is described. The energy resolution of the spectrometer improves with the square root of the intensity of the incident beam. It also increases linearly with the change in energy with respect to transmission efficiency of a particular foil. In theory, the resolution of the spectrometer can readily exceed 50 eV over a wide range of energies depending on the foils used and the incident X-ray photon flux. Determinations of the energies of Mo $K\alpha$ and Cu $K\alpha$ radiation using a first-generation ten-foil spectrometer gave values of 17.5 ± 0.1 and 8.08 ± 0.05 keV, respectively. Treatment of random error shows good correspondence with a Poisson model. The use of this spectrometer is demonstrated using a sample of tetraphenylphosphonium tetrachlorooxomolybdenum(V). Comparison of predicted and observed energies shows good agreement over a wide range of energies. The ratio of predicted to measured energy for the first 50 measurements was 0.9918 ± 0.0344. Up to three components of a position having harmonic overlap were separated. This work demonstrates the feasibility of using Laue diffraction to completely determine the crystal structure of a molecule without recourse to monochromatic methods.

Keywords: Laue diffraction; energy resolution; unit-cell determination; metal-foil spectrometer.

1. Introduction

Laue diffraction allows more of reciprocal space to be observed simultaneously than any other X-ray diffraction technique. However, the advantages of Laue diffraction go beyond the ability to observe large regions of reciprocal space. As a polychromatic X-ray technique it is inherently an experiment providing multiple anomalous dispersion. As a crystallographic method it is potentially the fastest method for the collection of data sets for structure determination (Coppens, 1992; Helliwell, 1992). Many of these capabilities are currently limited by existing instrumentation. As a general experiment for collection of data for structure determination it still provides many instrumental challenges. In particular, when faced with an unknown crystal, Laue diffraction at present is unsuitable for crystallographic structure determination. Such crystals are generally pre-examined using monochromatic techniques for the determination of unit-cell parameters and space groups (Helliwell, Gomez de Anderez, Habash, Helliwell & Vernon, 1989; Gomez de Anderez *et al.*, 1989). To date, only one method has been described for determining accurate unit-cell parameters using Laue data (Carr, Dodd & Harding, 1993; Carr, Cruickshank & Harding, 1992). Carr, Cruickshank & Harding (1992) used a crystal's gnomonic projection to determine axial ratios and then scaled the unit cell using a knowledge of λ_{min}. Variations on this method primarily involve ways of estimating λ_{min}. Approaches for evaluating the reflection intensities in multiple Laue diffraction spots have been described (Hao, Campbell, Harding & Helliwell, 1993; Campbell & Hao, 1993). These techniques have produced reasonable values at doubly overlapped spots. To date, space-group verification has not been demonstrated using these techniques. If instrumentation were available for the simultaneous determinations of position, intensity and energy, many of these procedures could be simplified

and perhaps complete structural determination of unknown crystals could be routinely performed using Laue diffraction data.

The Laue experiment has a variety of features that need to be considered. The spots observed typically appear at high spatial frequency requiring the detector to have a large number of elements, ideally over a large area. Each detected reflection contains energy information characteristic of the crystallographic plane that produced it. Some points in space contain multiple energies corresponding to overlapping orders of diffraction (Helliwell, 1992). The most demanding environment for the detection of energy-resolved Laue diffraction patterns is that found in synchrotron facilities where incident beam intensities are very high. The detector for this application needs to be able to cover a large area, have fast response at the energy of the spots, and be able to handle a large number of X-ray photons simultaneously. At present there is no high-resolution energy-resolved measurement system suitable for use with Laue diffraction at synchrotron facilities and little or no speculation has been made about how to produce such a system. If an area-detection system were available that allowed the determination of position, intensity and energy simultaneously, additional features of the Laue experiment could be unlocked. This paper describes the design and properties of a foil-mask spectrometer uniquely suited to Laue diffraction.

The foil-mask spectrometer for X-rays relies on wavelength modulation of the incident beam using a series of metal foils of varying composition and thickness. Modulation of the intensity of the resultant Laue diffraction image is encoded in a series of images taken through the foils measured in the intensity domain. These intensity domain images are then used to compute an energy image which could be used for determination of unit-cell parameters. The foil-mask spectrometer is capable of producing high-resolution energy measurements on the monochromatic reflections which make up the majority of reflections from the Laue diffraction pattern (Cruickshank, Helliwell & Moffat, 1991). These monochromatic reflections may be used to determine the unit-cell parameters. Knowing these parameters, the energies corresponding to reflections containing overlapping orders of diffraction can be predicted and the intensity of the overlapped orders can be determined for space-group assignment.

This paper describes the design, properties and limitations of such a spectrometer and discusses its application to Laue diffraction.

2. Principle of operation

2.1. *A foil-mask spectrometer: high-resolution energy determination of monochromatic X-rays*

A block diagram of a simplified spectrometer is illustrated in Fig. 1. The spectrometer works on the principle that materials absorb X-rays based on their elemental composition. Pure metal foils have an X-ray absorption spectrum characteristic of the thickness and electronic properties of the element composing the foil. Foils composed of alloys could also be used, but the presence of multiple K edges in the material would make subsequent analysis more complicated. The spectrometer consists of a series of foils arranged in a 'color wheel', an X-ray source and a detector. The foils are used to partially or completely 'mask' spectral regions in a predictable way. By modulating the incident beam in the energy domain, the energy information can be encoded in a series of measurements made with an energy-insensitive detector.

Let $T(\lambda)$* be the mathematical relationship between the transmission efficiency of a foil and the energy of the incident beam. In practice, this relationship is measured at particular wavelengths or may be computed from tabulated data.† When applied to Laue diffraction the incident polychromatic beam passes through a foil and is attenuated in an energy-dependent manner described by $T(\lambda)$ of the particular foil. The attenuated beam subsequently hits the crystal and is diffracted. The diffracted beams form a pattern of spots on an area detector. In a Laue diffraction pattern, the majority of these spots are created by monochromatic X-rays (Cruickshank, Helliwell & Moffat, 1991). A series of measurements of the intensity of the beam before and after each metal foil is placed in the beam are made. The transmission efficiency corresponding to each foil is evaluated and the energy of the X-rays is estimated by comparing the measured transmission effi-

* All symbols are defined in Table 1.

† All the tabulated data used in this paper are taken from Robinson (1974).

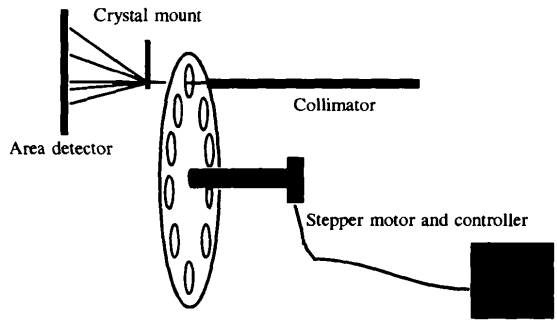

Figure 1
Schematic representation of a ten-element foil-mask spectrometer. Although not shown here, post-foil collimation must be applied. In this figure the elemental foils are introduced before the beam reaches the sample. While this arrangement is not required, it is advantageous. If the foil is placed after the crystal, a parallax correction must be applied to correct for the angle θ between the incident beam and the foil. Under such conditions the transmission efficiency for a given energy will be $T = \exp[-\mu(x/\cos\theta)]$, where x is the thickness of the foil, θ the angle of incidence and μ the linear absorption coefficient. This reduces the intensity rapidly at high angle and aggravates the $\sin(\theta)/\lambda$ fall-off in intensity in diffraction applications. For this reason the geometry illustrated here has been adopted.

Table 1
List of symbols.

$T(\lambda)$	Function relating the transmission of X-rays through a foil to the energy of the incident X-ray
$\mathbf{T}$	Row vector containing values of $T(\lambda)$ at particular energies
$\mathbf{T}_{el}$	$\mathbf{T}$ for a particular element, *e.g.* $\mathbf{T}_{Cu}$ contains values of $\mathbf{T}$ for the element copper
$\mathcal{T}$	Matrix consisting of n rows with each row corresponding to a different set of $\mathbf{T}$ values
$S(\lambda)$	Function relating the energy of an X-ray photon to the intensity of the X-ray source at that wavelength
$\mathbf{S}$	Column vector containing values of $S(\lambda)$ at particular energies
I	An intensity measurement made with an energy-insensitive detector on an X-ray beam after passing through a foil
$\mathbf{I}$	A column vector of intensity measurements passing through a set of foils as defined in a $\mathcal{T}$ matrix
θ	Angle of incidence between the foil mask and the X-ray beam
μ	Linear absorption coefficient
x	Foil thickness
T	Transmission efficiency of a foil mask at a particular energy, defined as the intensity after absorption divided by the incident intensity
ρ	Density

ciency with a set of tabulated transmission efficiencies in a look-up table containing transmission and energy. The energy or energies corresponding to this transmission efficiency are then reported. This process is illustrated in Fig. 2 for the case of a 50 μm Al foil.

A foil-mask spectrometer can be used in two ways. These include a high-resolution spectrometer for measuring the energy of a monochromatic source, or a low-resolution spectrometer for measuring the energy distribution of a polychromatic source. The first of these will be the focus of this paper; however, the theory describing the properties of the low-resolution spectrometer will be presented. The first is applicable to determining the energy of X-rays in monochromatic reflections from Laue diffraction.

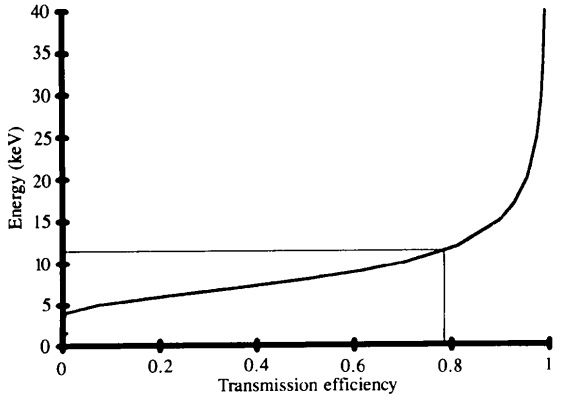

Figure 2
Illustration of the principle behind a foil-mask spectrometer. A measured transmission efficiency of 0.78 results in an energy of 12 keV. Data are for a 50 μm Al foil.

2.2. *Propagation of noise from the intensity domain into the energy domain*

The energy resolution of a foil-mask spectrometer is limited by the error in the determination of transmission efficiency and the derivative of the equation relating energy to transmission efficiency. Transmission efficiency is defined as:

$$T = I_{\text{mask}}/I_0. \tag{1}$$

The theoretical best case for the error in measurements of I_{mask} and I_0 is determined by Poisson statistics:

$$\sigma_{I_{\text{mask}}} = I_{\text{mask}}^{1/2}; \quad \sigma_{I_0} = I_0^{1/2}. \tag{2}$$

Propagating these errors into determination of T results in:

$$\sigma_t = [(1 + T)T/I_0]^{1/2}. \tag{3}$$

In this analysis it is assumed that the published tables of transmission efficiency and energy are well measured and do not represent a large source of error. The error defined by (3) then propagates by a factor of the derivative of the relationship between transmission efficiency and energy, $|dE/dT|$:

$$\sigma_E = |dE/dT|[(1 + T)T/I_0]^{1/2}. \tag{4}$$

This equation represents a theoretical best case for a system limited by Poisson noise. Other sources of error, such as source flicker or detector read noise, will degrade this performance.

Equation (4) has several consequences that allow the resolution of a foil-mask spectrometer to be optimized. First $|dE/dT|$ can be minimized by selection of foil thickness and composition. Second, the incident beam intensity, I_0, should be as large as possible. Selection of foils represents a compromise allowing a wide energy range to be measured. Fig. 3 shows the error function

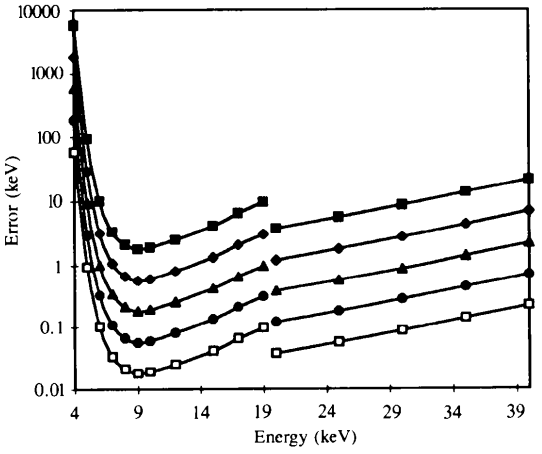

Figure 3
Plot of equation (4) for increasing values of I_0. Solid squares: $I_0 = 10$ photons; solid diamonds: $I_0 = 100$ photons; solid triangles: $I_0 = 1000$ photons; solid circles: $I_0 = 10\,000$ photons; open squares: $I_0 = 100\,000$ photons. Plot uses a 25 μm Nb foil. The discontinuity is due to the K edge of Nb.

defined by (4) plotted for increasing values of I_0 for a 25 μm Nb foil. Fig. 4 shows a plot of $|dE/dT|$ as a function of energy for Nb foils of varying thickness.

Equation (4) also assumes that the full width at half maximum (FWHM) of the energy distribution of the incident X-ray beam is much smaller than σ_E. The energy measured by the spectrometer shows a dependence on the FWHM. This dependence is complex and depends on the foil and the energy of the incident beam. Further development of this relationship will not be pursued here.

2.3. *A foil-mask spectrometer: low-resolution determination of broad-band X-ray sources having broad spectral features*

Using the definition of $T(\lambda)$ developed in §1, assume that $T(\lambda)$ is measured at n different values of λ. These values of T are stored in a row vector, **T**. If the incident intensity of an X-ray source as a function of λ is given by the function $S(\lambda)$, this can be represented as a column vector, **S**, when evaluated at known intervals. As is the case with $T(\lambda)$, in practice **S** is measured at particular wavelengths. The product of **T** and **S** gives the total intensity, I, of an X-ray beam after passing through a foil mask:

$$I = \mathbf{T} \cdot \mathbf{S}. \tag{5}$$

If many such masks are available then $T_{el}(\lambda)$, the transmission spectrum for each elemental mask, can be defined and the intensity of an X-ray beam passing through each mask can be computed. $\mathcal{T}$ is defined as a matrix, each row of which corresponds to a different mask and to the transmission efficiency at a particular wavelength interval:

$$\mathbf{I} = \mathcal{T} \cdot \mathbf{S}. \tag{6}$$

The quantity of experimental interest is **S**, the energy spectrum of the incident beam. **I** and $\mathcal{T}$ are the known quantities, while **S** is unknown. **S** can be determined by computing the inverse matrix $\mathcal{T}^{-1}$ and applying it to **I**:

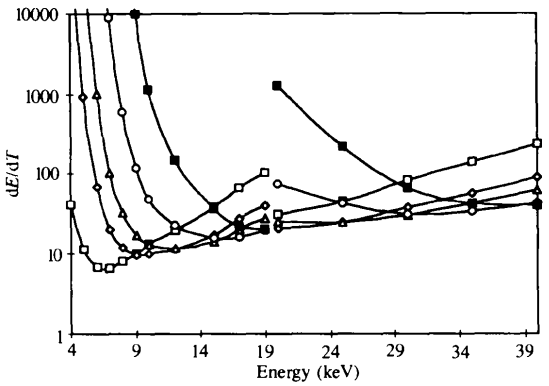

Figure 4
Derivative of the energy with respect to transmission efficiency for Nb foils of varying thickness. Open squares: 5 μm; open diamonds: 15 μm; open triangles: 25 μm; open circles: 50 μm; filled squares: 100 μm. Discontinuity is due to the Nb K edge. The thinnest foil allows for optimum resolution at low energies but the 5 μm foil has a limited range. 25 μm represents a compromise giving a wide range of utility.

$$\mathbf{S} = \mathcal{T}^{-1}\mathbf{I}. \tag{7}$$

Equation (7), which assumes that the inverse matrix $\mathcal{T}^{-1}$ can be computed, is a simplified expression defining a low-resolution X-ray spectrometer for polychromatic radiation. There are a number of limitations. First, as many masks must be employed as there are desired energy-resolution elements. Second, the spectral features must be broad relative to the width of each resolution element. Additionally, propagation of uncertainty is far more complex in this system than in the spectrometer for high-resolution measurements of monochromatic X-rays. In practice, use of a spectrometer of this type would probably require an over-determined multiple linear-regression approach to the data analysis since some foils will have near-zero transmission efficiency. While intriguing, such a spectrometer is of limited utility and will not be developed further here.

2.4. *Application to Laue diffraction*

The Laue experiment consists of an incident polychromatic beam of radiation. This polychromatic beam may come from either a laboratory-scale source or a synchrotron. While the incident beam is polychromatic, two features of the diffracted beams from the Laue experiment allow the application of the foil-mask spectrometer to the problem. First, the majority of reflections from the crystal produce monochromatic X-rays (Helliwell, 1992). Second, the remaining reflections either contain harmonic overlaps or spatial overlaps. The considerations in §2.2 are sufficient for measuring the position, energy and intensity of monochromatic reflections. The intensity of each component in a position containing harmonic or spatial overlap may also be treated using the foil-mask spectrometer provided the energies are previously known. In Laue diffraction, if the unit-cell parameters and the orientation matrix of a crystal are known, then the energies present in all spots may be computed. Knowing the energies present, the intensity of the spot may be partitioned among the energies present by setting up a system of linear equations. For example, let the incident beam contain X-rays with energies $\lambda_1, \lambda_2, \lambda_3, \ldots, \lambda_n$, let each harmonic component of the incident beam have intensity $H_{\lambda 1}, H_{\lambda 2}, H_{\lambda 3}, \ldots, H_{\lambda n}$, let $T_{m1}, T_{m2}, T_{m3}, \ldots, T_{mn}$ be the transmission efficiencies for masks $1, 2, 3, \ldots, n$, at $\lambda_1, \lambda_2, \lambda_3, \ldots, \lambda_n$, and let $I_1, I_2, I_3, \ldots, I_n$ be the measured intensities through each mask in the spectrometer. If the energies are known, this reduces to the following system of the linear equations:

$$\begin{bmatrix} I_1 \\ . \\ . \\ . \\ I_n \end{bmatrix} = \begin{bmatrix} T_{1,1} & . & . & . & T_{1,m} \\ . & & & & . \\ . & & & & . \\ . & & & & . \\ T_{n,1} & . & . & . & T_{n,m} \end{bmatrix} \begin{bmatrix} H_1 \\ . \\ . \\ . \\ H_n \end{bmatrix}. \tag{8}$$

It should be noted that these equations may also include the trivial case of no mask at all. A consequence of this set of equations is that the maximum number of harmonics which may be resolved into individual intensity components depends on the number of masks in the spectrometer. In practice, (8) will usually represent an over-determined system of equations and should be evaluated using standard statistical procedures. Additionally, these equations could presumably be used to resolve spatially overlapped reflections, those which are not sufficiently separated in space to be distinguished. Such conditions are common in proteins when the crystal-to-detector distance is small. Again this requires a knowledge of the spatial resolution of the detector system and computation of energy and position for the spatially overlapped reflections.

2.5. *Instrumental considerations – detectors*

The ideal detector for use within a foil-mask spectrometer would have unity gain at all energies and 100% quantum efficiency. While such a detector would be desirable, it is not a requirement. Detectors that might be used for this purpose are silicon-intensified targets (SITs) (Arndt, 1990; Li, Phillips, Stanton & Kalata, 1992), charge-coupled devices (CCDs) (Phillips, Li, Stanton, Xie & O'Mara, 1993; Allinson, 1989), charge-injection devices (CIDs) (Hanley, True & Denton, 1995), image plates (Miyahara, Takahashi, Amemiya, Kamiya & Satow, 1986), multiwire detectors, and even photographic film. It should also be noted that single-channel detectors such as avalanched photodiodes, GM counters, scintillation counters and ion chambers could also be used. Single-channel detectors incorporating a foil-mask spectrometer could be used as low-cost alternatives to Si(Li) detectors for assessing the amount of overlap in beams using multilayers for monochromation, particularly in very high flux environments.

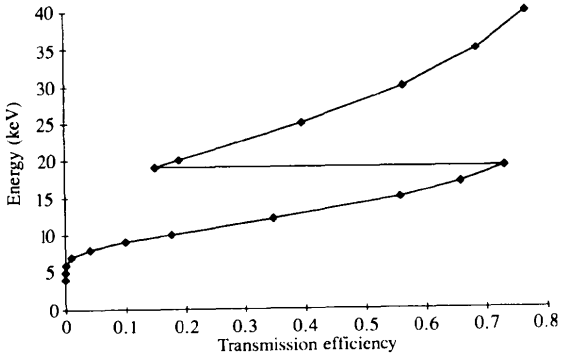

Figure 5
The region between a transmission efficiency of approximately 0.15 to 0.75 results in ambiguous values of energy due to the K edge of Nb. From data processing, the matches can be restricted to regions where $|dE/dT|$ is positive. This avoids the K edge. Selection from among the remaining two values is done by applying the criteria in §2.6. Data presented are for a 25 μm Nb foil.

Table 2
Foil compositions and thickness.

Element	Purity (%)	Nominal thickness (μm)	Measured thickness (μm)	Supplier	Single-valued area 4–40 keV*
Al	99.0	12.5	11.2	Goodfellow	Entire range
Al	99.5	25.4	25.4	Alfa	Entire range
Al	99.0	50	50.2	Goodfellow	Entire range
Ti	99.6+	15	16.2	Goodfellow	> 12.5 keV
Ni	99.5	25	25.0	Alfa	> 20 keV
Cu	99.9	12.5	13.2	Alfa	> 20 keV
Zr	99.99+	25	20.0	Alfa	< 8 keV
					> 19 keV
Nb	99.8	25	25.0	Alfa	< 8 keV
					> 38 keV
Mo	99.95	12.7	13.5	Alfa	< 9 keV
Ag	99.9	25	24.7	Alfa	$20 < E < 25.5$

* A 1 keV margin of error has been included when selecting these regions and the energy range has been restricted to 4–40 keV.

2.6. *Eliminating K-edge ambiguities in energy determinations*

Inclusion of elements having K edges in the range 4–40 keV results in ambiguity in the determination of the energy of the incident X-ray beam. A given transmission efficiency can result in three separate values for energy. This behavior is illustrated in Fig. 5. It is important to determine ways to eliminate K-edge ambiguities so as to obtain an unambiguous measurement of the energy of an incident beam of monochromatic X-rays. This may be done by selecting regions over which the transmission efficiency curve for a particular foil is single valued. Such regions are tabulated for the foils used here in Table 2.

A further problem is that reliable estimates of energy depend on good measurements of T. Foils for which the estimated error is large as predicted by equation (4) need to be excluded from the determination of energy. If a scintillation counter or multiwire detector is used, evaluation of the estimated error associated with a measurement may be made using (4). In other cases, a rough rule is to limit the use of foils where the transmission efficiency is less than 0.10 or greater than 0.80.

For a particular position in a measured Laue pattern, the transmission efficiency is first evaluated for each foil. The energy or energies corresponding to the measured transmission efficiency are computed, including ambiguous values. Energy values from each foil are evaluated in order of appearance in Table 2 to eliminate those outside the transmission efficiency criteria ($0.1 < T < 0.8$). The first foil meeting the criteria is used to set a target energy for eliminating K-edge ambiguities. If a K edge for a particular foil is within

Table 3
System operating conditions and crystal-system parameters.

Crystal	Tetraphenylphosphonium tetrachlorooxomolybdenum(V)
Crystal space group	$P4/n$*
Unit-cell parameters	$a = 12.7306$, $c = 7.6845$ Å*
X-ray source	Enraf–Nonius FR571 with Mo anode
Source voltage	50 kV
Source current	50 mA
Detector	CID38SG indirect camera system†
'Raster size'	176 μm
Image size	511 × 511

* Carducci (1994). † Hanley, True & Denton (1995).

0.8 keV of the target energy, then data from that foil is excluded. In the case of ambiguity, the value closest to the target energy is selected. Selected values meeting all of these conditions are averaged to obtain an initial estimate of the energy.

The initial estimate of the energy is refined using least-squares minimization of the difference between the measured and predicted transmission efficiencies. When a minimum is reached, the energy value is reported. The quality of the measurement of the energy is assessed using the final sum of squares.

3. Experimental

Foils of Cu, Ag, Al, Nb, Mo, Zr and Ni were obtained from Alfa Aesar (Ward Hill, MA). All remaining foils were obtained from Goodfellow (England). Specifications and purity of these foils are presented in Table 2. The thicknesses were measured by determining the transmission efficiency of the foil using Mo and Cu $K\alpha$ radiation.

Verification of equation (4) was made by making a series of measurements of I_0 and I for a monochromatic X-ray beam of known energy. A total of 25 values of transmission efficiency were obtained for each foil. The

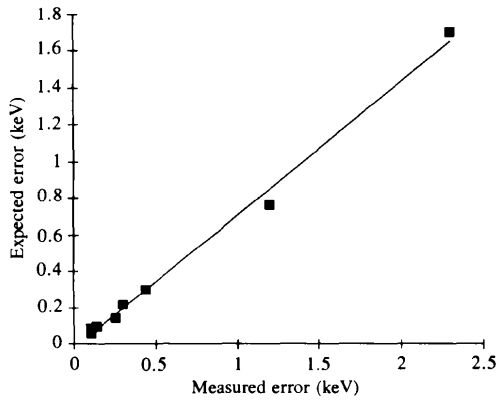

Figure 6
Plot of expected random error *versus* measured random error for eight foils measuring Mo $K\alpha$ X-rays. The thinnest Al foil and the Zr foil are excluded from this plot: see text for details. Slope of the line is 0.73 ± 0.06. True error is slightly degraded from the theoretical best case. In all cases the value of I_0 was approximately 45 500 counts.

Table 4
Error comparison for eight foils measuring Mo $K\alpha$ X-rays.

Foil	Estimated random error*	Measured random error†	Systematic error‡
Al 25.4	1.7	2.3	1.38
Al 50	0.76	1.2	0.91
Ti 15	0.30	0.46	−0.03
Ni 25	0.058	0.11	−0.36
Cu 12.5	0.095	0.14	−0.19
Nb 25	0.14	0.25	0.39
Mo 12.7	0.21	0.30	0.17
Ag 25	0.087	0.11	0.12

* Random error estimates were computed using equation (4) and the measured I and I_0. † The standard deviation of a series of energy measurements is reported as measured random error. ‡ The difference between the literature value of Mo $K\alpha$ radiation and the mean value of a series of measured energies is reported as systematic error.

energy was computed for each of the foils at each individual measurement of transmission efficiency. The reported measured random error is the standard deviation of the series of measurements through each foil. The predicted error was computed based on I_0, I and equation (4). The X-ray source in these experiments was a sealed-tube Mo source followed by a graphite monochromator. The $0\bar{1}0$ reflection from 2-dimethylsulfuranylidene-1,3-indandione (Christensen & Thom, 1971) was used to produce an X-ray source of appropriate intensity. The difference between the literature value for the Mo $K\alpha$ radiation and the mean value of energy measured with each foil is reported as systematic error.

A series of Laue diffraction images of tetraphenylphosphonium tetrachlorooxomolybdenum(V) were taken using an indirect charge-injection-device camera system previously described (Hanley, True & Denton, 1995). Exposures were taken with and without the foils attenuating the incident beam. X-rays were generated using an Enraf–Nonius FR571 rotating-anode X-ray source with an Mo anode. The unfiltered direct beam was used to generate the Laue diffraction pattern. The system operating

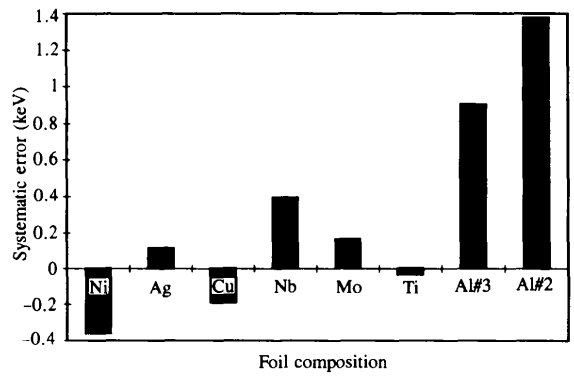

Figure 7
Systematic errors for each of the foils in preceding figure. Under the conditions of measurement the Al foils would be excluded due to the large expected error based on the Poisson model. Under conditions where the number of counts is unknown, T should be constrained between 0.10 and 0.8.

conditions and the crystal-system parameters are outlined in Table 3. The orientation of the crystal was found and refined using the program *LAUEGEN* (Campbell, 1995). Prediction of the energies present at locations of known index were made using the simulation option of *LAUEGEN*. Additional image processing was performed using the image reduction and analysis facility (*IRAF*) written by the National Optical Astronomical Observatories (NOAO) running on a Sparc Station II (Sun Microsystems). Peak search and integration was performed using the *IRAF PHOT* subprogram. Separation of harmonic overlaps into component intensities was performed using multiple linear regression with stepwise inclusion of components having P values less than 0.05. Since each integrated value was background corrected, the regressions were forced to include the origin. This analysis was made using the *SPSS* computer program (SPSS, Inc., Chicago).

4. Results

4.1. *Calibration*

The measured X-ray thickness of each foil is given in Table 2. The results of a comparison of expected random error and measured random error in determinations of the energy of Mo $K\alpha$ radiation are plotted in Fig 6. The 12.5 μm Al foil and the 25 μm Zr foil do not appear in this figure. The 12.5 μm Al foil does not attenuate the beam sufficiently. The 25 μm Zr foil, while significantly attenuating the beam, has a K edge very close to the Mo $K\alpha$ emission energy. This results in poor estimates of energy. Systematic errors for these same foils are charted in Fig. 7. The data for expected random error, measured random error and systematic error are tabulated in Table 4. The average energy using all foils meeting the criteria outlined in §2.6 is 17.5 ± 0.1 (s.e.) keV, remarkably close to the literature value of 17.48 keV. Similar measurements made using Cu $K\alpha$ gave a value of 8.08 ± 0.05 (s.e.) keV, again close to the literature value of 8.05 keV.

Table 5
Refined parameters for the Laue diffraction pattern of Fig. 8.

Orientation	
Phix	91.80°
Phiy	3.51°
Phiz	107.89°
Refined detector characteristics	
Crystal-to-detector distance	68.99 mm
X center	237.4
Y center	243.1
'Twist'	44.589 (0.01°)
'Tilt'	75.578 (0.01°)
'Bulge'	17.516 (0.01°)

4.2. *Crystal orientation and pattern indexing*

Fig. 8 is the I_0 Laue diffraction pattern image taken of tetraphenylphosphonium tetrachlorooxomolybdenum(V). The center of the pattern was found using conic centering. Twenty reflections were selected interactively using *LAUEGEN* and the orientation of the difraction pattern was found based on the known unit-cell parameters and crystal class. The orientation angles, crystal-to-detector distance and detector parameters (bulge, tilt and twist) were further refined after entry of 156 reflections matching the simulated pattern. Refined parameters are summarized

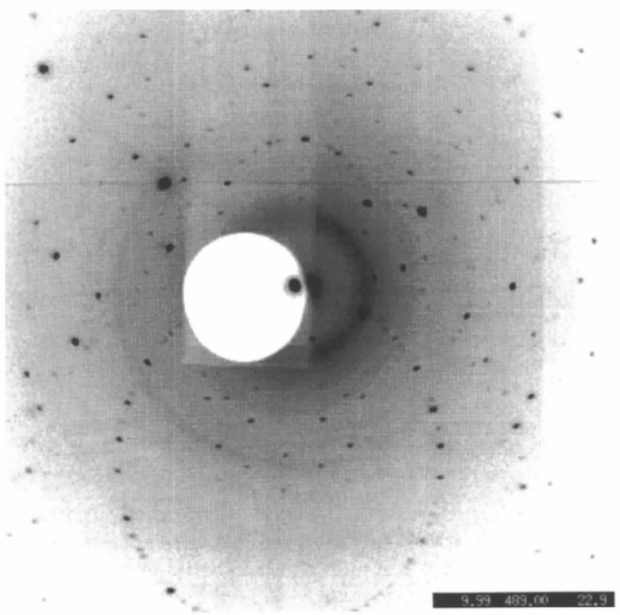

Figure 8
The I_0 Laue diffraction pattern image of tetraphenylphosphonium tetrachlorooxomolybdenum(V).

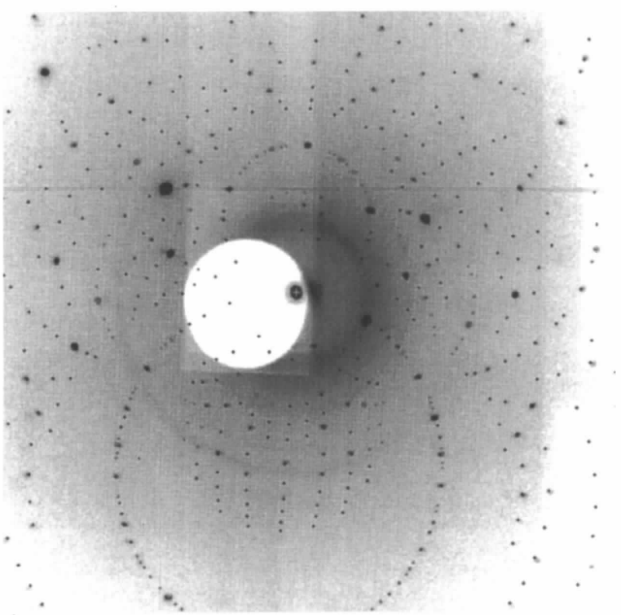

Figure 9
The predicted pattern of Fig. 8 superimposed on the observed image.

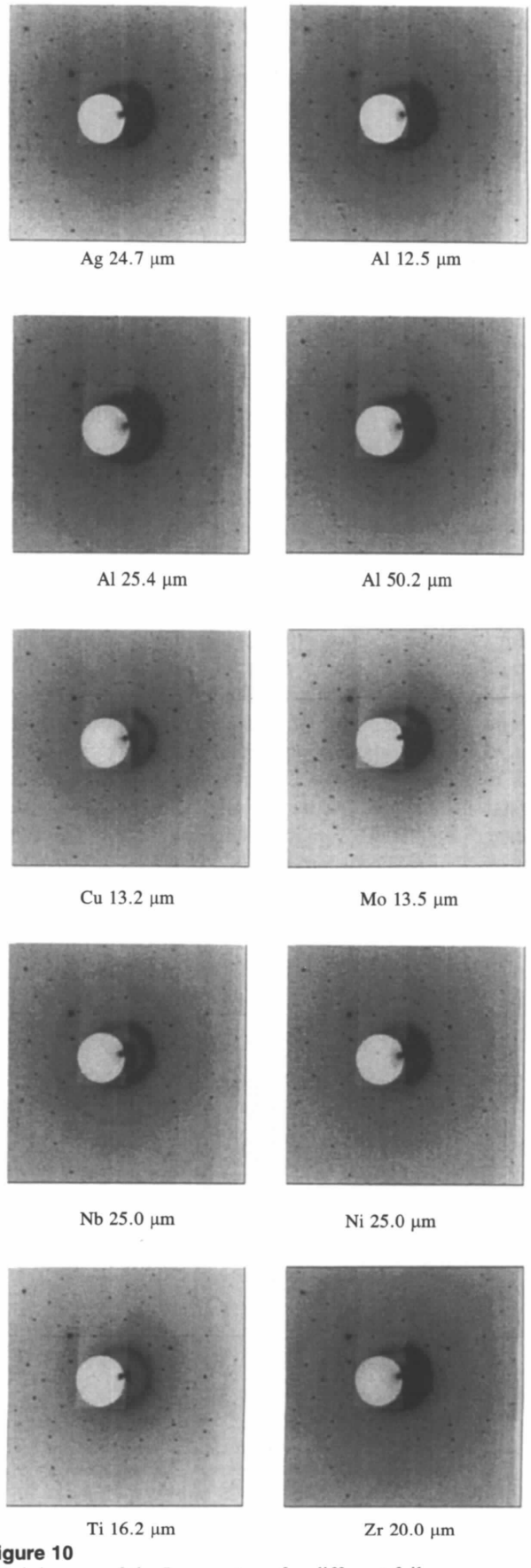

Figure 10
Mask images of the Laue pattern for different foils.

in Table 5. Fig. 9 shows the predicted pattern superimposed on the observed image. Energies for observed reflections consisting of monochromatic or harmonic overlaps were simulated using *LAUEGEN* based on the refined orientation.

Eleven images of the Laue pattern were measured. Each corresponded to one of the foil masks or the I_0 image. The ten mask images are shown in Fig. 10. The spots in the image were selected interactively using *IRAF* and the intensities integrated. Energy analysis was attempted on a total of 118 positions, regardless of the existence of multiple harmonic overlaps. Of these 118 positions, 92 were predicted to be monochromatic.

4.3. *Monochromatic energy comparison*

Using the simulated pattern the reflections containing monochromatic components were selected. The 92 reflections were sorted in order of increasing sum of squares as defined in §2.6. These were divided in half with the best 46 and the worst 46 in separate groups. The two groups are plotted against the predicted energy in Fig. 11. The ratio of

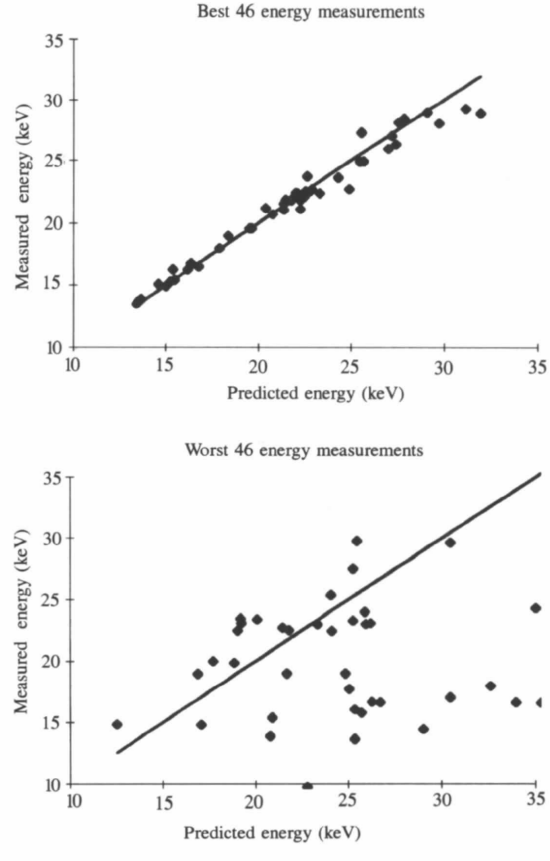

Figure 11
Correspondence between predicted and measured energy for best and worst measurements of monochromatic reflections. Measurement quality is assessed using the squared difference between the predicted transmission efficiency and measured transmission efficiency. Correspondence degrades rapidly as the sum of squares exceeds 0.2. The line in each figure is for ideal 1:1 correspondence.

Table 6
Regression analyses for each type of harmonic overlap.

Harmonic type	(h, k, l)	Energy	Intensity	Significance
Double	$(\bar{1}, 1, 3)$			
		10.8	1694 ± 304	0.0003
		21.6	643 ± 237	0.0237
Regression statistics:	$R^2 = 0.977$	$F = 196$	Significance <0.0001	
Degrees of freedom	Regression = 2		Residual = 9	
Triple	$(\bar{1}, \bar{1}, \bar{2})$			
		9.27	431 ± 94	0.0018
		18.54	451 ± 134	0.0099
		27.80	428 ± 121	0.0080
Regression statistics:	$R^2 = 0.994$	$F = 452$	Significance <0.0001	
Degrees of freedom	Regression = 3		Residual = 8	
Quadruple	$(\bar{1}, \bar{2}, \bar{1})$			
		10.57	3159 ± 145	<0.0001
		21.14	5295 ± 217	<0.0001
		31.71	1224 ± 170	0.0001
		42.28	—	Not significant
Regression statistics:	$R^2 = 0.999$	$F = 12{,}203$	Significance <0.0001	
Degrees of freedom	Regression = 3		Residual = 8	
Sextuple	$(1, 1, \bar{1})$			
		5.61	—	Not significant
		11.23	—	Not significant
		16.84	4046 ± 172	0.0000
		22.45	4263 ± 173	0.0000
		28.07	—	Not significant
		33.68	—	Not significant
Regression statistics:	$R^2 = 0.999$	$F = 15{,}126$	Significance <0.0001	
Degrees of freedom	Regression = 2		Residual = 9	

predicted to measured energy is 0.993 ± 0.034 for the best group and 0.767 ± 0.298 for the worst group.

4.4. *Harmonic overlaps*

Harmonic overlaps were present in 26 of the observed spots. The estimated number of harmonics present in these spots ranged from 2 to 6. Of the 26 positions predicted to contain harmonic overlap, 14 were doubles, 4 were triples, 6 were quadruples and 2 were sextuples. Regression analyses for each type of overlap are summarized in Table 6. Further analysis was not made since the wavelength normalization curve for the detector system is unknown.

5. Discussion

5.1. *Calibration*

Figs. 6 and 7 demonstrate the potential of the foil-mask spectrometer system. Random errors show a clear correlation with equation (4). This shows the resolution of the spectrometer is predictable and can be optimized by increasing the incident X-ray flux and decreasing the value of $|dE/dT|$. With a high incident flux, the random error of the energy measured with a foil-mask spectrometer decreases by the square root of the intensity. The value of the slope of measured error *versus* expected error is 0.73. It is unclear why the slope differs from unity.

At present, systematic errors vary depending on the foil. Several factors may account for these errors in the present spectrometer system. First, a linear interpolation algorithm was used between points giving some inherent error to the computed values of energy. Second, impurities in the foils will result in systematic errors in computed energies. Finally, the measured X-ray thicknesses represent the average of the values obtained using Mo and Cu $K\alpha$ radiation. As such they represent a compromise. Future systems should seek to calibrate the transmission efficiency of the foils at a variety of energies rather than relying on published values of μ/ρ as was done here. For example, the transmission efficiency could be measured every 50 eV, resulting in improved energy estimates. Despite these limitations, the average value of energy using these foils is remarkably close to the literature values reported for both Mo and Cu $K\alpha$ radiation.

5.2. *Monochromatic energy comparison*

The data presented in Fig. 11 show that the performance of the spectrometer on images is degraded somewhat from the results obtained for monochromatic Cu and Mo $K\alpha$ sources. The first 50% of the data show excellent agreement with the predicted values. The sum of squares used to refine the energy values appears to be a good *a priori* index of data quality. For the system described here, the energy values can be considered reliable provided the sum of squares is kept under 0.2. After this point is reached, the quality of the data degrades rapidly. While it is justifiable to exclude values when the sum of squares gets large, it is more desirable to improve the measurements of transmission efficiency. A sum of squares value

of 0.2 obtained from ten separate masks represents an average disagreement of 0.045 transmission efficiency units. Further development of the technique should be able to improve these measurements considerably. A reasonable target for future systems is to measure all the transmission efficiencies to better than 0.02 transmission efficiency units. This criteria is currently being met by only four of the monochromatic spots. If this criteria were to be met, the final sum of squares would be less than 0.05. Reaching this level of precision might bring an added benefit by being able to separate spots containing harmonic overlap from monochromatic spots on *a priori* considerations.

5.3. *Harmonic overlaps*

The data in Table 6 show the capability of separating multiple components of a spot containing harmonic overlap using the system of foil masks. The major components of the overlapped positions can be separated and an error assigned. The data presented here are primarily for demonstration purposes since the wavelength normalization curve of the detector is not known. Without further characterization of the detector the 'true' relative intensities cannot be verified. Future work in this area should allow this to be tested in more detail.

The method for separation of intensity components containing harmonic overlap described here is similar to the *UNSCRAM* procedure previously described (Helliwell, Habash *et al.*, 1989). *UNSCRAM* applies to the use of stacked absorbers (between films in a pack) for unscrambling the intensity components in overlapped spots. The *UNSCRAM* procedure is general to any system of stacked calibrated absorbers between detecting elements.

While *UNSCRAM* is most applicable to the use of film as a detector, the analysis described here is general to all systems of absorbers. The instrumental adaptation described has a number of advantages. It is computationally simplified since no parallax correction is needed, a condition which is unavoidable in film systems. It avoids the problems involved in the use and digitization of film images. The use of a solid-state detector allows for the possibility of real-time assessment of image quality. The system of foils only needs to be calibrated once. In the case of film each lot must be calibrated separately. Finally, since the method is not dependent on a particular detector, the 'color wheel' may be physically removed and installed with another detection system without loss of calibration.

6. Conclusions

There are several features of the foil-mask spectrometer described here that are attractive for Laue diffraction, particularly at synchrotron facilities. The spectrometer is robust with respect to radiation damage, components are inexpensive to replace, and the method is general to any area detector currently in use. It is well suited to modern solid-state camera systems. Unlike energy-dispersive detectors, the energy resolution of a foil-mask spectrometer improves with the square root of the incident beam intensity. Si(Li) detectors and CCDs used as direct X-ray detectors have degraded performance at high incident-beam intensities. The foil-mask spectrometer is adaptable to detection systems ranging from single-channel scintillation counters to large-format CCDs. The primary fundamental limitation of the foil-mask spectrometer system is that it requires multiple exposures.

For Laue diffraction, combining crystallographic refinements and position and energy measurements from a foil-mask spectrometer should allow complete determination of the space group and unit-cell parameters of an unknown crystal. The procedure consists of first determining the energy of each of the monochromatic reflections in the Laue diffraction pattern. These measurements of position and energy can be used to deduce the unit cell of the unknown crystal. Once these are known, the energies that should be present in reflections containing overlapping orders of diffraction can be computed. Knowing the energies that must be present, a set of linear equations can be set up to measure the intensities of overlapping reflections. In conventional Laue diffraction, such information is not available and prior monochromatic examination of crystals is necessary.

Considerable development of the foil-mask spectrometer system is still needed. There are three main areas needing improvement. First, improving the precision of measurements of transmission efficiency will allow a greater portion of observed spots to be used for later unit-cell determination. Second, a detection system needs to be characterized sufficiently to allow wavelength normalization to be applied to the collected data. Finally, automated image processing needs to be applied to allow convenient extraction of peaks from an image. When these problems are solved the spectrometer system may be useful for full crystallographic structure determination using Laue diffraction.

The long-term goal of this research is to develop instrumentation allowing complete structure and space-group determination using a single instrument and Laue diffraction. Such instrumentation requires the development of area detectors with high energy resolution. The foil-mask spectrometer meets many of the required properties of such an instrument. Further development should allow more widespread use of the Laue diffraction method.

The authors would like to thank Dr William Montfort, Dr Sue Roberts and Dr Michael Bruck for assistance with the X-ray generators, Colin Earle for invaluable computing assistance with *IRAF* and *LAUEGEN*, and Dr John Enemark for suggesting the Laue diffraction application. We are particularly indebted to Dr John Campbell of Daresbury Laboratory, UK, for the use of, and assistance with, *LAUEGEN*. This research was supported by a monetary grant from

Thermo-Jarrell-Ash corporation and material donations from CID Technologies.

References

Allinson, N. M. (1989). *Nucl. Instrum. Methods,* **A275**, 587–596.
Arndt, U. W. (1990). *Synchrotron Radiat. News,* **3**(4), 17–22.
Campbell, J. W. (1995). *J. Appl. Cryst.* **28**, 228–236.
Campbell, J. W. & Hao, Q. (1993). *Acta Cryst.* A**49**, 889–892.
Carducci, M. (1994). Personal communication.
Carr, P. D., Cruickshank, D. W. J. & Harding, M. M. (1992). *J. Appl. Cryst.* **25**, 294–308.
Carr, P. D., Dodd, I. M. & Harding, M. M. (1993). *J. Appl. Cryst.* **26**, 384–387.
Christensen, A. T. & Thom, E. (1971). *Acta Cryst.* B**27**, 581–586.
Coppens, P. (1992). *Synchrotron Radiation Crystallography.* New York: Academic Press.
Cruickshank, D. W., Helliwell, J. R. & Moffat, K. (1991). *Acta Cryst.* A**47**, 352–373.
Gomez de Anderez, D., Helliwell, M., Habash, J., Dodson, E. J., Helliwell, J. R., Bailey, P. D. & Gammon, R. E. (1989). *Acta Cryst.* B**45**, 482–488.
Hanley, Q. S., True, J. B. & Denton, M. B. (1995). *J. Synchrotron Rad.* **2**, 215–228.
Hao, Q., Campbell, J. W., Harding, M. M. & Helliwell, J. R. (1993). *Acta Cryst.* A**49**, 528–531.
Helliwell, J. R. (1992). *Macromolecular Crystallography with Synchrotron Radiation.* Cambridge University Press.
Helliwell, J. R., Habash, J., Cruickshank, D. W. J., Harding, M. M., Greenhough, T. J., Campbell, J. W., Clifton, I. J., Elder, M., Machin, P. A., Papiz, M. Z. & Zurek, S. (1989). *J. Appl. Cryst.* **22**, 483–497.
Helliwell, M., Gomez de Anderez, D., Habash, J., Helliwell, J. R. & Vernon, J. (1989). *Acta Cryst.* B**45**, 591–596.
Li, Y., Phillips, W. C., Stanton, M. & Kalata, K. (1992). *Nucl. Instrum. Methods*, A**332**, 116–125.
Miyahara, J., Takahashi, K., Amemiya, Y., Kamiya, N. & Satow, Y. (1986). *Nucl. Instrum. Methods*, A**246**, 572–578.
Phillips, W. C., Li, Y., Stanton, M., Xie, J. & O'Mara, D. (1993). *Nucl. Instrum. Methods*, A**334**, 621–630.
Robinson, J. W. (1974). Editor. *Handbook of Spectroscopy*, Vol. 1. Cleveland, Ohio: CRC Press.